1-1-2019

A new class of bubble-free water electrolyzer that is intrinsically highly efficient

Prerna Tiwari
University of Wollongong, pt832@uowmail.edu.au

George Tsekouras
University of Wollongong, georget@uow.edu.au

Klaudia K. Wagner
University of Wollongong, kwagner@uow.edu.au

Gerhard F. Swiegers
University of Wollongong, swiegers@uow.edu.au

Gordon G. Wallace
University of Wollongong, gwallace@uow.edu.au

A new class of bubble-free water electrolyzer that is intrinsically highly efficient

Abstract

A new class of 'bubble-free' alkaline electrolyzer with electrodes comprising of PTFE-based Gortex gas diffusion layers coated with catalysts, is described (PTFE = poly(tetrafluoroethylene)). At ≥80 °C (Eocell 1.18 V), the electrolyzers displayed the lowest cell onset potentials (≥1.28 V) yet reported, indicating that they exhibit the highest-known intrinsic efficiency when the influence of impedance is stripped out. The overpotentials at each electrode, particularly the oxygen-generating anode, were significantly diminished by the presence of the porous Gortex substrate, which exhibited a powerful 'gas-philic' capillary action (6.3 bar capillary pressure). The bubble-free process arose from preferential coalescence of newly-formed gases on the PTFE surfaces, where the capillary action of the Gortex continuously extracted them before they could nucleate bubbles. In so doing, observable bubble formation was avoided, along with the energy penalties associated with the formation and release of gas bubbles.

Disciplines

Engineering | Physical Sciences and Mathematics

Publication Details

Tiwari, P., Tsekouras, G., Wagner, K., Swiegers, G. F. & Wallace, G. G. (2019). A new class of bubble-free water electrolyzer that is intrinsically highly efficient. International Journal of Hydrogen Energy, 44 (42), 23568-23579.

A New Class of *Bubble-Free* Water Electrolyzer that is Intrinsically Highly Efficient

Prerna Tiwari, George Tsekouras, Klaudia Wagner, Gerhard F. Swiegers,[*] Gordon G. Wallace

Intelligent Polymer Research Institute, University of Wollongong, Wollongong, NSW 2522, Australia and ARC Centre of Excellence for Electromaterials Science, University of Wollongong, Wollongong, NSW 2522, Australia

ABSTRACT: A new class of "bubble-free" alkaline electrolyzer with electrodes comprising of PTFE-based Gortex gas diffusion layers coated with catalysts, is described (PTFE= poly(tetrafluoroethylene)). At ≥80 ^{o}C (E^{o}_{cell} 1.18 V), the electrolyzers displayed the lowest cell onset potentials (≥1.28 V) yet reported, indicating that they exhibit the highest-known intrinsic efficiency when the influence of impedance is stripped out. The overpotentials at each electrode, particularly the oxygen-generating anode, were significantly diminished by the presence of the porous Gortex substrate, which exhibited a powerful '*gas-philic*' capillary action (6.3 bar capillary pressure). The bubble-free process arose from preferential coalescence of newly-formed gases on the PTFE surfaces, where the capillary action of the Gortex continuously extracted them before they could nucleate bubbles. In so doing, observable bubble formation was avoided, along with the energy penalties associated with the formation and release of gas bubbles.

KEYWORDS: electrolysis, Gortex, overpotential, water-splitting, hydrogen

1. INTRODUCTION

A future hydrogen economy based on renewable energy will, undoubtedly, be critically dependent on efficient water electrolysis.[1,2] Electrolyzers split water according to the overall reaction:[1]

$$2\ H_2O + \text{electrical energy} + \text{heat} \rightarrow O_2\ (g)\ (\text{anode}) + 2\ H_2\ (g)\ (\text{cathode}) \quad ...(1)$$

While the *equilibrium voltage* (E^o_{cell}) for the above reaction is 1.23 V at 25 °C (1.18 V at 80 °C),[1] no modern electrolyzer is capable of operating near to this potential. This is illustrated by Figure 1, which compares the best reported polarization curves for the major classes of electrolyzers at

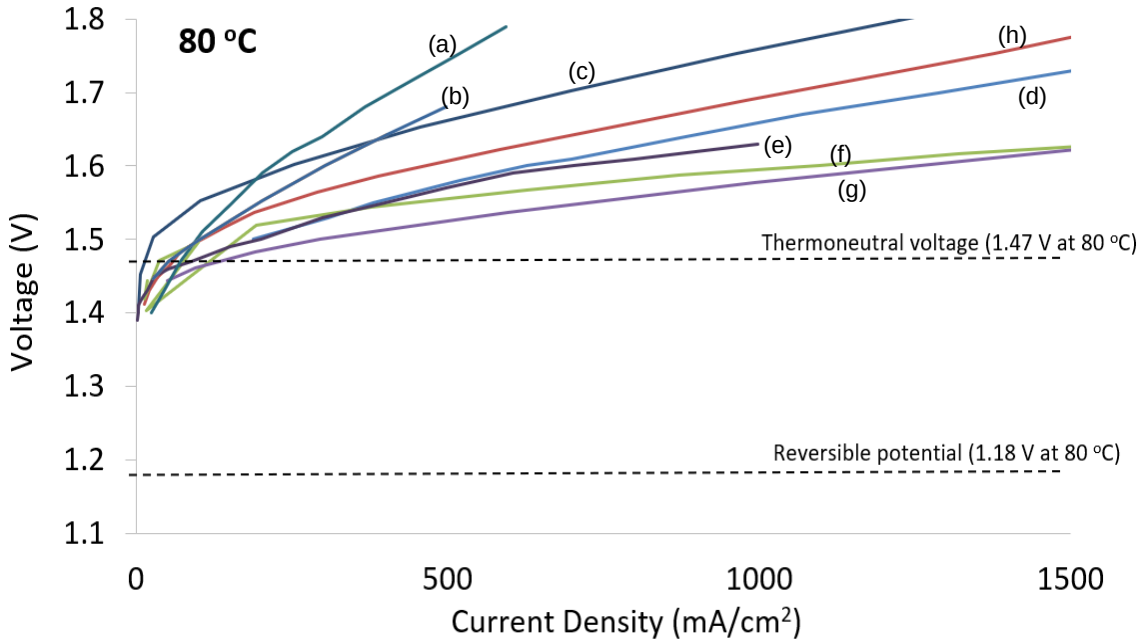

Figure 1. The best reported polarization curves at 80 °C and atmospheric pressure, for: (a)-(b) alkaline electrolyzers;[2,6] (c)-(g) PEM electrolyzers with inter-electrode ionomer membranes of thickness: (c) ~183 μm,[7] (d)-(e) ~125 μm,[8,9] (f)-(g) ~50 μm;[7,10] and (h) alkaline exchange membrane electrolyzer.[11]

80 ^{o}C and atmospheric pressure, namely: (1) alkaline electrolyzers (Figures 1(a)-(b)); (2) proton exchange membrane (PEM) electrolyzers, incorporating inter-electrode ionomer membranes of thickness: (i) ~183 μm (e.g. Nafion 117; Figure 1(c)), (ii) ~125 μm (e.g. Nafion 115; Figures 1(d)-(e)), (iii) ~50 μm (e.g. Nafion 212; Figures 1(f)-(g)); and (3) alkaline exchange membrane electrolyzers (Figure 1(h)). As can be seen, gas generation commences, in all cases, near to the *thermoneutral voltage* (E_{TN}) (1.47 V at 80 ^{o}C; 1.48 V at 25 ^{o}C) and not E_{cell}^{o}.[1] E_{TN} is the potential at which the heat produced electrically matches that required in reaction (1). Below E_{TN}, heat must be supplied (e.g. by extraction from the surroundings). Above E_{TN}, excess heat is generated and radiated.[1]

All of the electrolyzers further exhibit onset potentials of ≥1.45 V (Table S1; Figure S1). The onset potential is formally the y-axis intercept of a straight-line fit of the ohmic region of the polarization curve.[3] Onset potentials provide a measure of the intrinsic efficiency of electrolyzers, when the effect of cell architecture is stripped out. The lowest of the onset potentials in Figure 1 are those of the alkaline electrolyzer in Figure 1(b) (1.45 V) and the PEM electrolyzers in Figures 1(d) and 1(g) (1.46 V and 1.45 V, respectively) (Table S1; Figure S1). The diversity of this grouping indicates that the onset potentials (≥1.45 V) are not influenced by whether the electrolysis is acidic or alkaline. Instead, they must be associated with another feature that is common to these electrolyzers.

One such feature is that they all produce gases in the form of bubbles. The energy required to form and release gas bubbles (the "*bubble overpotential*") is believed to contribute to the high onset potentials.[4,5] This has, for example, been used to explain why electrolysis of seawater (pH 8.4) yields chlorine gas, Cl_2 (E^{o} 1.36 V) at the anode instead of the thermodynamically more

favored O_2 gas (E^o 1.23 V).[5] But, precisely how large this contribution may be has never been determined experimentally because of the difficulty of splitting water without bubble formation. In this work we examine the effect of eliminating observable gas bubble formation on the onset potential of water electrolysis.

Another outcome of gas bubble formation is that an ion-permeable, gas-impermeable membrane must be incorporated between the electrodes. This is needed to keep the hydrogen bubbles produced at the cathode from mixing with the oxygen bubbles generated at the anode and vice versa.[1] A hydrogen stream containing >4.6% O_2 or an oxygen stream comprising >3.8% H_2 is potentially explosive at 80 ^oC.[1]

A key disadvantage of such membranes is their low conductivity, which is, at best, ~0.17 S/cm for hydrated Nafion and ~0.4 S/cm for commercial alkaline Zirfon membranes at 80 ^oC (*vs.* >1.35 S/cm for 4.5 M H_2SO_4 and 6 M KOH).[12] This limitation has driven cell design, with all of the above electrolyzers employing *zero-gap* architectures in which the electrodes are tightly sandwiched on opposite sides of the inter-electrode membrane.[13] This arrangement minimizes the *impedance* of the cell, which is the opposition that the cell circuit presents to a current when a voltage is applied. Specifically, *zero-gap* architectures diminish the *area specific resistance (ASR)* of the cell and thereby minimize the ohmic slope of the polarization curve.[13] The best electrolyzers display slopes (ASRs) of ~100 mΩ cm^2 (Table S1; Figure S1).

If gas can be formed and collected directly, without the need to produce and release gas bubbles, then the requirement for an ion-permeable, gas-impermeable membrane between the electrodes may potentially be done away with. This work also examines the

effect of eliminating observable gas bubble formation on the need for an inter-electrode membrane.

We report impedance-*un*optimized *"bubble-free"* alkaline electrolyzers that safely produces gases without observable bubble generation and without a membrane between the electrodes. One such electrolyzer, which employed gas diffusion electrodes comprising of micro-porous, hydrophobic *Gortex* substrates layered with Raney-Ni at the cathode and $NiCo_2O_4$ at the anode, displayed an onset potential of only 1.28 V at 80 ^oC. This corresponds to an iR-corrected cell overpotential of only 90 mV and derived from declines in the electrode overpotentials at $\geq$80 ^oC induced by the Gortex. The overpotential at the anode $NiCo_2O_4$ catalyst at 10 mA/cm^2 at 80 ^oC, fell from ~0.27 V without the Gortex present, to a mere 0.11 V with the Gortex present; a 0.16 V decline. This exceeded the overpotential decline of 0.09 V induced by a thin, hydrophobic, nano-porous polyethylene substrate that was reported during the drafting of this publication.[14] In that system, the overpotential for O_2-generation at a $Au/NiFeO_x$ catalyst at 10 mA/cm^2 fell from 0.28 V without the substrate to 0.19 V with the substrate.[14]

Newly-formed gases are well-known to preferentially coalesce on PTFE surfaces, like those of the Gortex. The absence of observable bubbles at each electrode was explained by these gases being continuously drawn into the Gortex before they nucleated bubbles. The Gortex displays a powerful '*gas-phillic*' capillary action (6.3 bar capillary pressure). By contrast, in conventional "bubble-generating" electrocatalysis the liquid electrolyte must be continuously supersaturated to high levels with dissolved gas in order to nucleate and release a stream of gas bubbles.[15]

The above onset potential, which is the lowest yet reported, indicates that the *bubble overpotential* may constitute a notable energy contribution in water electrolysis, equivalent to ≥11.9% LHV. Stripping out the effect of impedance, the above electrolyzer is, to the best of our knowledge, the most intrinsically efficient ever reported.

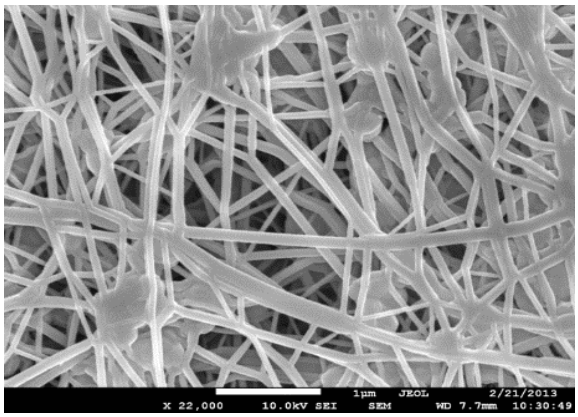

Figure 2. Scanning electron micrograph of the ePTFE surface of an uncoated Gortex membrane showing Teflon fibrils.

2. RESULTS AND DISCUSSION

2.1 Gortex Gas Diffusion Layers in '*Bubble-Free*' Water Electrolysis. *Gore-Tex*, a brand name supplied by the W. L. Gore company, or its generic version '*Gortex*', comprises of a ~20 μm thick porous membrane of microscopically-small Teflon filaments (known as *expanded PTFE*, or *ePTFE*) (Figure 2), supported by a thicker, fibrous polypropylene backer.[16,17] The *ePTFE* membrane in Gortex is highly permeable to gases, however its strong hydrophobicity blocks the passage of aqueous liquids.[18] This has led to its application as a textile for example, where it allows water vapor from a wearer's body to pass through it, but not liquid rain that may fall on it. For

similar reasons, Gortex has also been widely used to extract dissolved gases from liquids in industry.[19]

Gortex has been examined as a gas diffusion layer in several electrochemical cells.[18,20-24] In 2012, Winther-Jensen and co-workers in our research center studied Gortex as a novel *Gas Diffusion Layer (GDL)* in the electrodes of a water electrolysis cell.[20] A thin, conductive and catalytic Pt layer was sputter-coated onto Gortex strips, which were then employed as gas diffusion electrodes at both the anode and cathode. The Gortex electrodes were found to generate H_2 and O_2 gases without evident bubble formation, as observed through the transparent walls of an acrylic test cell and measured with gas probes.[20] An ion-permeable, gas-impermeable diaphragm/ionomer between the electrodes did not appear to be necessary in the absence of bubbles.

The 'bubble-free' nature of the electrolysis was attributed to the gases being produced at or very close to the liquid-solid-gas interface, meaning that it was more efficient for them to pass across that interface into the Gortex than to form bubbles. Bubble nucleation requires fairly extreme supersaturation of the electrolyte with the gas in order to achieve the very high partial pressures needed (>14 atm for O_2 bubbles with a 0.1 μm radius at 25 ^{o}C).[20]

Unfortunately, the presence of the Gortex substrate also imparted a high hydrophobicity upon the thin, sputter-coated layer of Pt, making it a poor catalyst. Current densities beyond 10 mA/cm^2 were not easily achieved. The effect of bubble-free water splitting at higher current densities could therefore not be assessed.

In following up this work, we were, accordingly, interested to develop Gortex-based electrodes coated with thicker and more hydrophilic layers of catalysts that could achieve high current densities in bubble-free water electrolysis.

A potential complication became apparent however, from work published shortly thereafter by Villa and colleagues, who built and studied the first water electrolyzers with conventional carbon-PTFE gas diffusion electrodes at both the anode and cathode.[25] These electrodes employed thick, hydrophilic catalyst layers of the type we were interested in. During operation at atmospheric pressure, some bubbles were, however, generated at the electrodes.[25] This was likely because some gas was produced too far away from the solid-liquid-gas interface within the catalyst layer; the conventional carbon-PTFE gas diffusion layers were unable to extract this gas.[25] The bubble formation could, however, be apparently suppressed by applying a 2 bar overpressure to the liquid electrolyte (relative to the gas chambers).[25] While this caused electrolyte to leak unsustainably into the gas chambers, the electrolyzer could be characterized, at least initially. It displayed the lowest cell onset potential recorded at that time at 80 ºC: 0.42 V.[25]

A key challenge in developing bubble-free Gortex electrodes with thick, hydrophilic catalyst layers, was therefore to come up with a design that eliminated the possibility of gas bubble formation, even at atmospheric pressure.

2.2 Designing a "*Bubble-Free*" Electrode with a Thick, Hydrophilic Catalyst Layer. A potential solution to this problem was provided by a 1987 patent that taught the fabrication of porous chlor-alkali electrodes which produced gas bubbles only on their back side, facing away from the counter-electrode.[26] Such electrodes comprise of two layers, as depicted in Figure 3(a):

- *Layer 1*: a *conductive*, hydrophilic, porous layer with small average pore size; and
- *Layer 2:* a thinner, *non-conductive*, chemically inert (refractory oxide) layer that was also hydrophilic and porous with small average pore size. *Layer 2* is adhered to the front side of *Layer 1*, facing its counter electrode.

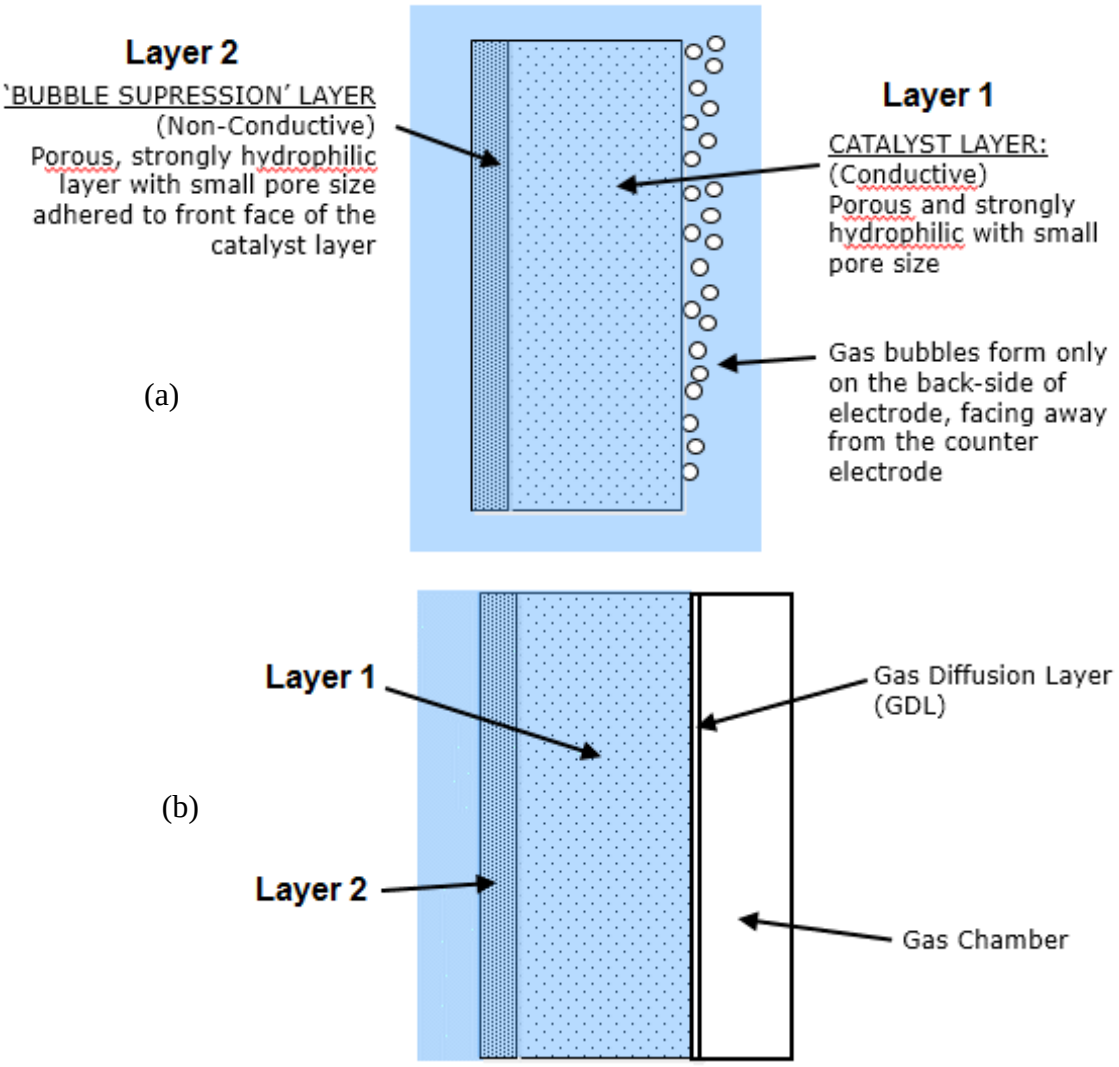

Figure 3. Schematic depiction of: (a) a porous electrode that generates gas bubbles only on the side facing away from the counter electrode, and (b) modification of the above electrode to directly generate gas without bubble formation (i.e. a '*bubble-free*' gas-generating electrode).

Because of their fine pore structure and hydrophilic character, capillary actions draw in and 'hold' aqueous electrolyte within each of *Layer 1* and *Layer 2*. The resulting capillary pressure impedes bubble nucleation because it increases the internal pressure (known as the Laplace pressure)[27] that is required to create and expand a gas bubble. That is, gas bubbles forming within *Layers 1* and *2* not only have to push water out of the way during their expansion, but also have to overcome the capillary pressure with which that water is held in the pores.

As gases are only produced electrochemically by the conductive *Layer 1*, the role of the non-conductive *Layer 2* is simply to impede gas bubble formation on the surface of *Layer 1* facing the counter electrode. That is, bubble formation at the front surface of *Layer 1* is disfavored by the capillary pressure of the attached *Layer 2*. For this reason, *Layer 2* is termed a "*bubble-suppression layer*" in Figure 3(a).

Gas bubbles are therefore only favored to nucleate on the back surface of *Layer 1*, facing away from the counter electrode (Figure 3(a)), where they can expand into open solution without having to overcome a capillary pressure.

An electrode of this type should be readily modified to be totally bubble-free in its operation, by merely affixing a porous gas diffusion layer with an associated gas chamber, to the bubble-generating surface, as depicted in Figure 3(b). That is, an electrode of the type in Figure 3(a) should be readily converted into a gas diffusion electrode of the type in Figure 3(b) that directly produces a gas from a liquid electrolyte without the intermediacy of gas bubble formation.

In order to operate effectively, the capillary pressure within *Layer 1* of such an electrode must be high enough that gas bubbles don't have the opportunity to form inside it. That, in turn, depends on the capacity of the gas diffusion layer to continuously *de-gas* the liquid electrolyte inside *Layer 1* to thereby maintain its level of gas supersaturation below that required for bubble formation. If these two, inter-dependent properties can be simultaneously realized in an electrode, then sustained, direct gas generation, without bubble formation, should be possible.

2.3 The Gortex Electrodes and Electrolyzer Cells of this Study. Given these insights, we coated Gortex membranes (0.2 μm average pore diameter) with tightly compressed catalyst layers

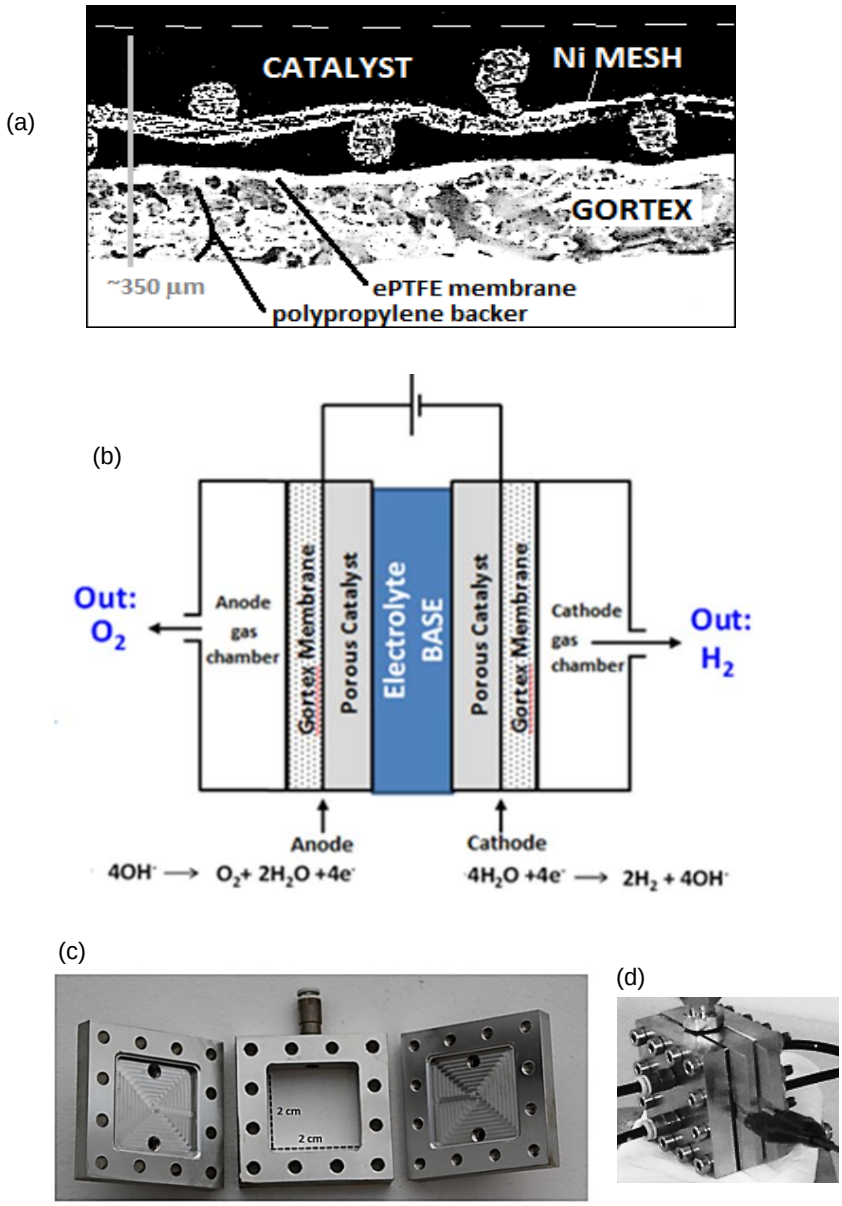

Figure 4. (a) Cross-section of a typical catalyst-coated Gortex electrode, showing the *ePTFE* membrane with polypropylene backer at the bottom and the Ni mesh and catalyst layer at the top. The dashed line at the top of the image depicts the surface of the catalyst layer. (b) Schematic depiction of the electrolyzer, showing the Gortex electrode with porous catalyst layer ('BASE' = 6 M KOH); (c)-(d) Photographs of the cell before and after assembly.

containing PTFE as a binder and a fine Ni mesh as a current carrier. The Supplementary Material describes the techniques employed to fabricate the electrodes, which included a compression step to create a finely pored catalyst layer. Raney Ni or 10% Pt on Vulcan XC72 ('10% Pt') was

employed as the cathode catalyst and $NiCo_2O_4$ as the anode catalyst. Figure 4(a) depicts a representative cross-section of the electrodes. As described in a previous publication,[18] Gortex-based gas diffusion electrodes of this type are highly permeable to gases (4 L min^{-1} cm^{-2} bar^{-1}) but *leak-proof* in respect of penetration by aqueous electrolyte (water entry pressures of ~5.7 bar).

When tested as working electrodes in transparent, acrylic cells, the Gortex electrodes, thus fabricated, did not produce observable gas bubbles on their surfaces during water-splitting up to at least 50 mA/cm^2 at atmospheric pressure (and, in some cases, up to 150 mA/cm^2). This indicated that the Gortex strongly de-gassed the catalyst layer. The Supplementary Material provides a video showing the surface of a representative Gortex electrode at various current densities (Video S1). For comparative purposes, ingress of gas through the Gortex was blocked in a small section of the electrode in the video (indicated with an arrow), forcing the formation of gas bubbles in that region.

Application of a 0.3-1.5 bar overpressure on the liquid electrolyte (relative to the gas chambers) allowed for very much higher current densities without observable bubble formation. Because of the leak-proof nature of the Gortex, aqueous electrolyte was excluded from the gas chambers. Still higher current densities could be realized, bubble-free, by also tightly covering the surface of the Gortex electrode with a bubble-suppression layer in the form of a thin, porous, polyethersulfone microfiltration membrane (Supor®, 0.45 μm average pore diameter, supplied by Pall Corporation). Current densities of ≥1000 mA/cm^2 (and as high as ≥2700 mA/cm^2) could be achieved.

Figure 4(b) schematically depicts the electrolyzer cell used to study these electrodes. As can be seen, three interchangeable components were combined to make up the cells: two gas collecting half-cells (Figure 4(c) left and right) and a central separator unit that created the inter-electrode gap (Figure 4(c) center). Electrodes could be interchangeably incorporated into the cell

which maintained them in a parallel, facing disposition to each other (Figure 4(b); Figures S2-S4). The space between the electrodes, was filled with 6 M KOH solution and did not incorporate an ion-permeable, gas-impermeable diaphragm/ionomer. Inter-electrode separations of 10 mm, 5 mm and 3 mm were available (and produced similar onset potentials with different ohmic slopes). A central separator unit comprising transparent, polished acrylic was also available, allowing us to video the inter-electrode volume and the surface of the electrodes during operation.

Immediately prior to testing, the gas chambers of the electrolyzer were flushed with pure H_2 (cathode) or O_2 (anode), or with inert N_2, in order to avoid any unwanted side-reactions (e.g. an O_2-depolarization reaction in which air oxygen in the cathode gas chamber is consumed).

To maintain a constant 80 ^oC temperature, the cell was submerged in a stirred, temperature-controlled, water bath during data collection. The sealed nature of the cell ensured that its gaseous and liquid contents did not contact or mix with the surrounding water.

For consistency, the data reported below was measured at atmospheric pressure with a 10 mm inter-electrode gap, without pressure differentials and without a bubble suppression layer over the Gortex electrodes. Gas bubbles were not observed in the inter-electrode space or on the electrode surfaces.

2.4 Safety Considerations in the Electrolyzer. The Need for an Ion-Permeable, Gas-Impermeable Diaphragm/Ionomer between the Electrodes. Prior to operating a new class of electrolyzer, it is essential to evaluate as fully as possible, the potential safety risks deriving from gas crossover between the electrodes. In the case of the present electrolyzer, we initially established that the individual Gortex electrodes did not produce gas bubbles during water-electrolysis. In the absence of bubbles and with a significant inter-electrode gap (10 mm)

containing a static liquid electrolyte and no diaphragm/ionomer, the only possible mode of crossover was diffusion of dissolved gases in the 6 M KOH electrolyte. We therefore modelled the crossover using Fick's law of diffusion.

At 80 ^{o}C, H_2 and O_2 are very poorly soluble in 6 M KOH, with equilibrium saturation concentrations of ~0.0000976 mol/kg (H_2) and ~0.0000876 mol/kg (O_2).[28] They also have exceedingly small diffusion coefficients of ~0.0000592 cm^2/s (H_2) and ~0.0000198 cm^2/s (O_2).[29,30] Accordingly, Fick's law predicts negligible levels of diffusion-based crossover between the electrodes. At a (bubble-free) current density of 10 mA/cm^2 with a 10 mm inter-electrode gap that does not include an inter-electrode diaphragm/ionomer, the crossover was calculated to be 0.0083% O_2 in the H_2 stream and 0.0137% H_2 in the O_2 stream. This equates to a predicted H_2 purity of >99.992% and an O_2 purity of >99.986% (not considering water vapor). At higher current densities (and/or lower temperatures), these already trivial crossovers decline still further. Smaller inter-electrode gaps increase the crossover, which, nevertheless, remains small. Even with an inter-electrode gap as small as 0.1 mm, crossover at ≥10 mA/cm^2 (80 ^{o}C; 6 M KOH) is well within the safety limits (<2% H_2 in the O_2, or O_2 in the H_2). Details of the above calculations are provided in the Supplementary Material.

These results are many orders of magnitude lower than the crossover in conventional PEM and alkaline electrolyzers, which cannot be safely operated below ~100-350 mA/cm^2.[31-33]

Gas crossover under bubble-free conditions, without a diaphragm/ionomer between the electrodes, therefore did not seem to constitute a potential safety hazard. Subsequent experiments with actual bubble-free electrolyzers (described below) confirmed very low crossover that appeared consistent with the modelling. It, consequently, seems that inter-electrode diaphragms/ionomers are redundant and unnecessary in bubble-free water electrolysis.

2.5 Chronopotentiograms and Faradaic Efficiency. Studies now turned to examining the Gortex electrodes in the electrolyzer cell shown in Figure 4(b)-(d). To eliminate artefacts and possible sacrificial/side reactions, the electrodes were initially pre-conditioned at 10 mA/cm^2 for 1 h at 80 ^{o}C. Their polarization curves were then measured, also at 80 ^{o}C.

The most remarkable data for the pre-conditioning step was obtained when a Gortex anode coated with $NiCo_2O_4$ (26.2 mg/cm^2), PTFE (16.7 mg/cm^2) and a Ni mesh ('$NiCo_2O_4$+PTFE+Ni-mesh/Gortex') was combined with a Gortex cathode coated with Raney Ni (38.8 mg/cm^2), carbon black (CB) (2.4 mg/cm^2), PTFE (15.2 mg/cm^2) and a Ni mesh ('Raney Ni+CB+PTFE+Ni-mesh/Gortex'). Another highly active combination involved the above anode combined with a cathode comprising of Gortex coated with 10% Pt on Vulcan XC72 (0.071 mg Pt/cm^2), carbon black (2.1 mg/cm^2) and PTFE (2.1 mg/cm^2), with a Ni mesh current collector ('10% Pt/CB+PTFE+Ni-mesh/Gortex').

These electrolyzers required a cell voltage of ≤1.31 V to generate 10 mA/cm^2 over 1 h at 80 ^{o}C. Figure 5 depicts a representative chronopotentiogram. This stands in stark contrast with the conventional electrolyzers in Figure 1, which needed ≥1.40 V to produce 10 mA/cm^2.[6-11,25]

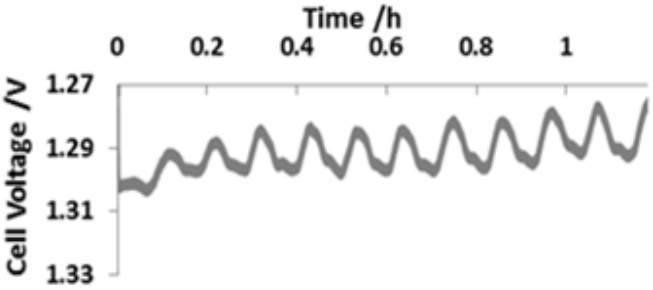

Figure 5. Representative two-electrode chronopotentiogram at 10 mA/cm^2 of a bubble-free electrolyzer operating at ~80 ^{o}C and comprising of 10% Pt/CB+PTFE+Ni-mesh/Gortex (cathode) and $NiCo_2O_4$+PTFE+Ni-mesh/Gortex (anode). Electrolyte: 6 M KOH.

The periodic fluctuations in the measured voltage in Figure 5 were observed in all of the chronopotentiograms. While puzzling at first, it later became apparent that they derived from temperature swings (~5 ^{o}C) in the water bath as the heater-controller struggled to maintain 80 ^{o}C in the face of strong cooling by the cell, which was operating far below the thermoneutral voltage. As predicted by theory, the cells vigorously extracted heat from their surroundings during operation. Without the cell present, the heater controller had no difficulty maintaining a constant temperature in the water bath.

To establish whether the 10 mA/cm^2 current was due to water electrolysis, the gas generated by the cathode was collected for 40 min in an upturned 5 mL burette filled with water, in a second water bath. The experimental setup had previously been developed and calibrated to quantify the volume and purity of H_2 collected by a Gortex-based H_2-extraction cell.[22]

At 10 mA/cm^2, a water electrolysis cell with 100% Faradaic efficiency should produce 3.04 mL of H_2 at the cathode over 40 min. In our work, ~2.99 mL of hydrogen was collected, which equated to a Faradaic efficiency of 98.4%. The collected gas was also confirmed to be pure hydrogen using an attached gas chromatograph (GC). To the limit of detection (<99.9% H_2 purity), O_2 could not be detected in the H_2 collected.

It could be concluded that the gas crossover in the cell was comparable to that predicted by Fick's law of diffusion. The high Faradaic efficiency also ruled out side-reactions.

2.6 Polarization Curves. The polarization curve of the Raney-Ni/$NiCo_2O_4$ electrolyzer, measured at 80 ^{o}C after the above pre-conditioning step, was also remarkable in several ways.

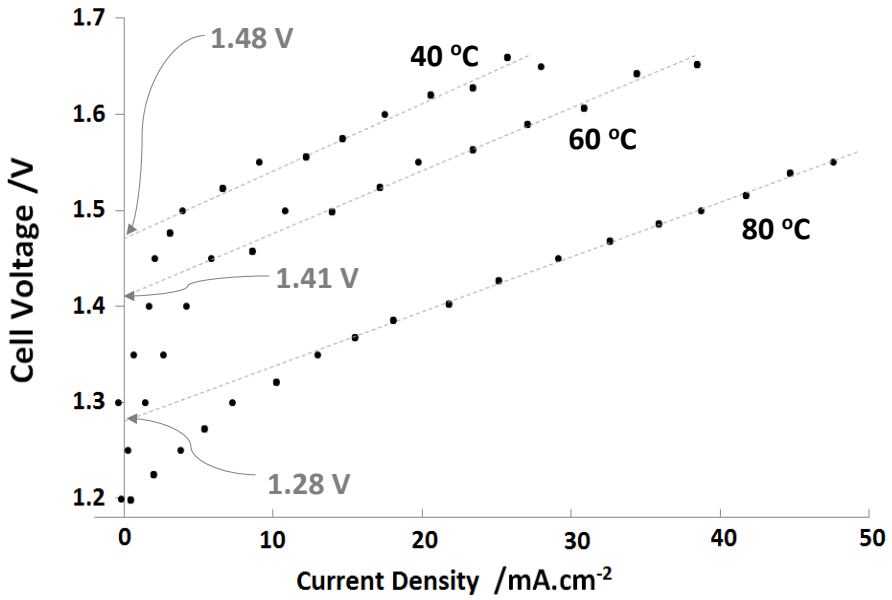

Figure 6. Polarization curves under bubble-free conditions at different temperatures after conditioning for 1 h at 10 mA/cm^2 and 80 °C, for the Raney Ni+CB+PTFE+Ni-mesh/Gortex (cathode) and $NiCo_2O_4$+PTFE+Ni-mesh/Gortex (anode) electrolyzer (6 M KOH electrolyte). The arrows mark the onset potential at each different temperature.

The most notable feature was the onset potential, which was a mere 1.28 V (Figure 6). The iR-corrected onset potential, which excludes the ohmic losses of the electrolyte (0.0074 V)[12] and the resistance of the Ni mesh (5.67 x 10^{-7} V), was 1.27 V. These values are well below the onset potentials of the electrolyzers in Figure 1 (≥1.45 V)[6-11,25] and also closer to the equilibrium potential for water electrolysis, E^o_{cell} (1.18 V at 80 °C).[34]

The difference between E^o and the onset potential of a water electrolyzer is formally termed its *activation overpotential*, η^{act}_{cell}.[1] The above, bubble-free electrolyzer exhibited an η^{act}_{cell} of 0.09 V. This includes the activation overpotential at both the anode and cathode. To the best of our knowledge, this is the lowest η^{act}_{cell} ever reported for a water electrolyzer. The smallest activation overpotential of the bubble-generating electrolyzers in Figure 1 is η^{act}_{cell} 0.27 V (Table S1),[2,10] which is 0.18 V higher than that of the bubble-free electrolyzer. This result indicates that the bubble-free electrolyzer was significantly more efficient than the bubble-generating electrolyzers

at the point at which current started being generated; that is, before impedance affected performance.

Polarization curves at 60 ^{o}C and 40 ^{o}C were also measured. As can be seen in Figure 6, at 60 ^{o}C (E^{o}_{cell} 1.20 V),[34] the onset potential was 1.41 V, which corresponded to a η^{act}_{cell} of 0.21 V. At 40 ^{o}C (E^{o}_{cell} 1.21 V),[34] the onset potential was 1.48 V, which equated to a η^{act}_{cell} of 0.27 V.

The large change in the onset potential from 40 ^{o}C to 80 ^{o}C is unusual. To the best of our knowledge, the onset potential of water electrolyzers are normally relatively unaffected by temperature. For example, the onset potential of the electrolyzer in Figure 1(a) changed by only 0.04 V in going from 40 ^{o}C to 80 ^{o}C.[6] The strong temperature dependence of the Gortex electrolyzer suggested a different catalytic mechanism that is more sensitive to temperature.

Figure 6 further shows that, at 80 ^{o}C, the current-voltage curve became significantly flattened and closer to linear. The 'dogleg' due to activation, that is highly characteristic of electrolyzer polarization curves, can be seen to become more linear at 80 ^{o}C. This is also unusual. To the best of our knowledge, near-linear curves that pass close to the equilibrium potential have previously only been observed in steam electrolyzers.[1]

A last unusual feature was the abbreviated activation region at 80 ^{o}C. As can be seen in Figure 6 the polarization curve, effectively, flattened to linear, ohmic behavior above ~15 mA/cm^2. In conventional electrolyzers, activation typically continues up to, at least, 100 mA/cm^2, with the ohmic region only commencing thereafter, at higher current densities (Figure S1).

2.7 Independent Verification and Similar Effects in Previously-Studied Electrolyzers.

Because of the unusual nature of the above observations, we had comparable tests carried out independently. The tests were performed at another laboratory using a different high-performing

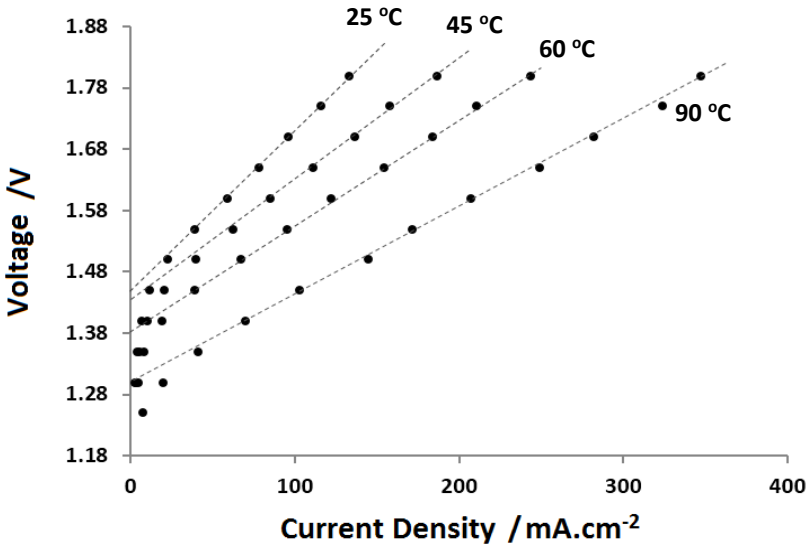

Figure 7. Polarization curves at different temperatures after conditioning for 1 h at 10 mA/cm^2 and 80 °C, for the bubble-free electrolyzer with plasma-nano-Ni+CB+PTFE+Ni-mesh/Gortex (cathode) and Plasma-nano-Ni+PTFE+Ni-mesh/Gortex (anode) (6 M KOH electrolyte). The original data, which was collected in quadruplicate, is provided in Figure S5.

catalyst layered on Gortex. The catalyst, which was employed at both the anode and cathode, was a plasma-generated nanoparticulate Ni ('plasma-nano-Ni') (average particle size: ≤20 nm). The electrolyzer cell in which it was tested had an inter-electrode gap of 5 mm and also did not incorporate a diaphragm/ionomer between the electrodes. These tests, which are described in the Supplementary Material, produced the polarization curves in Figure 7. As can be seen, they exhibit all of the same key features seen in the above work; namely:

(i) an onset potential that declined sharply with increasing temperature (to 1.30 V, with η^{act}_{cell} 0.11 V, at 90 °C);

(ii) a systematic flattening of the current-voltage curve to near-linearity at ≥80 °C; and

(iii) an abbreviated activation region (≤20 mA/cm^2).

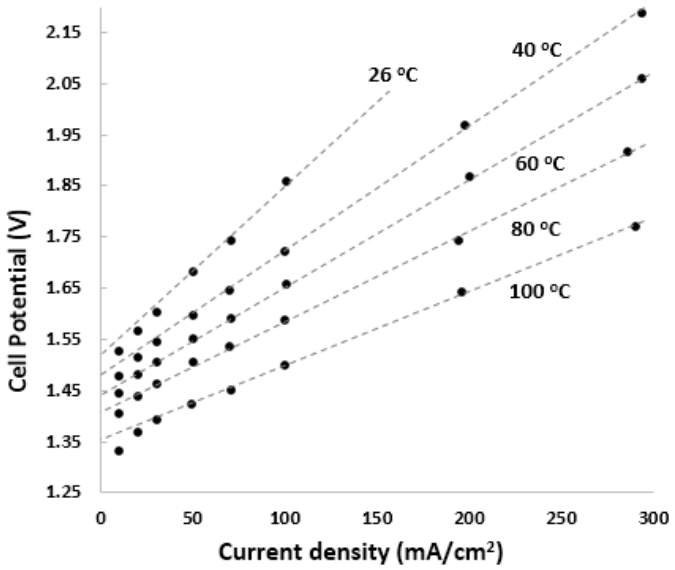

Figure 8. Polarization curves of the previously reported Villa electrolyzer,[7] which employed conventional carbon-PTFE-based gas diffusion electrodes with the 6 M KOH electrolyte overpressured by 2 bar (relative to the gas chambers) in order to eliminate gas bubble formation. The original data is provided in Figure S6.

Another electrolyzer that displayed these trends, albeit less intensely, was the earlier-mentioned alkaline electrolyzer of Villa and co-workers,[25] which employed two conventional, (non-Gortex) carbon-PTFE gas diffusion electrodes under conditions where bubble formation was suppressed. Figure 8 depicts its polarization curves when a 2 bar overpressure was applied to the liquid electrolyte (relative to the gas chambers). Under these bubble-free conditions, the electrolyzer displayed:[25]

(i) a notable decline in the onset potential with increasing temperature (to ~1.35 V, η^{act}_{cell} ~0.17 V, at 100 °C),

(ii) a flattening of the current-voltage curve to more nearly linear at ≥80 °C; and

(iii) an abbreviated activation region (<~30 mA/cm^2).

These results suggest that the above effects are not unique to Gortex electrodes. They may be general to the use of gas diffusion electrodes as a class, and merely amplified when Gortex is

used as the gas diffusion layer. Clearly, the nature of the gas diffusion layer plays an important role in decreasing the onset potential at temperature ≥80 °C.

2.8 The Origin of the Decline in Onset Potential. To examine the origin of the temperature-induced decline in the onset potential, we studied the electrolyzer of Figure 6 in a 3-electrode arrangement. A miniature Ag/AgCl reference electrode was incorporated in the inter-

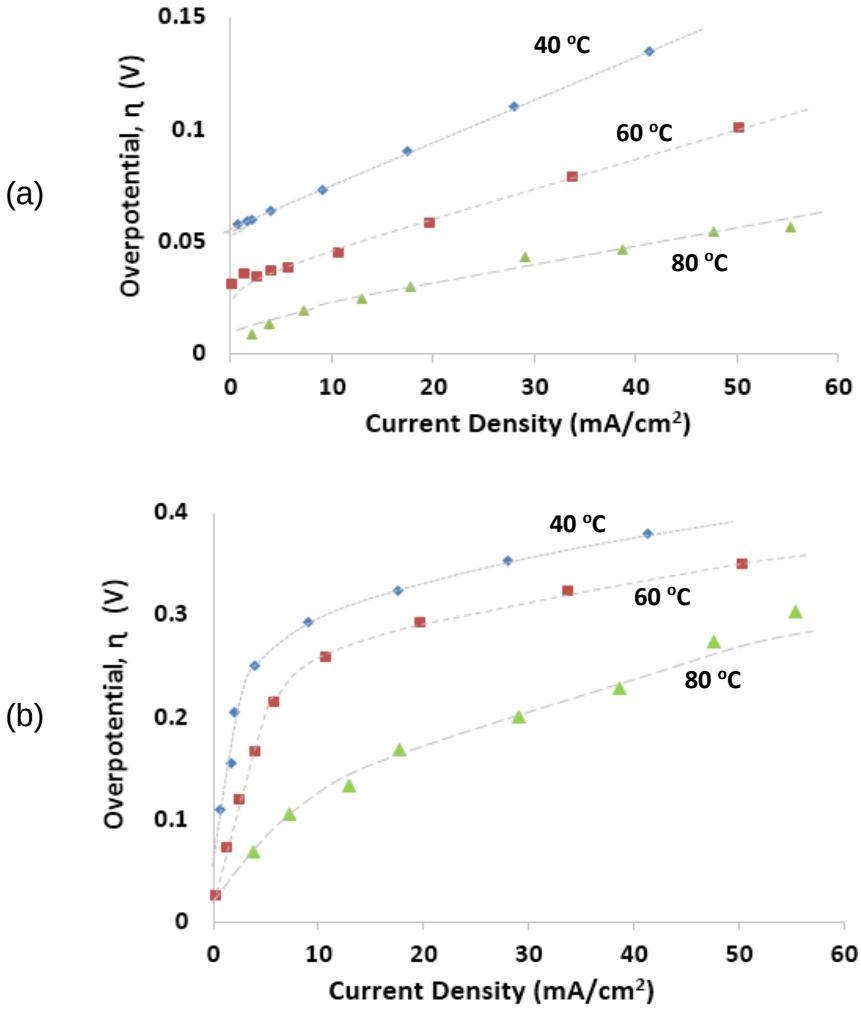

Figure 9. Overpotential as a function of current density and temperature under bubble-free conditions for the Raney Ni+CB+PTFE+Ni-mesh/Gortex (cathode) and $NiCo_2O_4$+PTFE+Ni-mesh/Gortex (anode) electrolyzer (6 M KOH electrolyte; 80 °C) at: (a) the hydrogen-generating cathode, and (b) the oxygen-generating anode.

electrode space and two potentiostats were used to monitor the voltage at each of the cathode and anode at 40-80 ^{o}C. As the equilibrium potential at the anode and cathode may be calculated for the electrolyte pH and temperature using the Nernst equation, the overpotential at each could be determined as a function of current density.

Figure 9 depicts these overpotentials at the different temperatures. As can be seen in Figure 9(a), the overpotential of cathodic H_2 generation under bubble-free conditions at 10 mA/cm^2 was ~70 mV at 40 ^{o}C. This is of similar order to previous reports[28] in which H_2 was produced in the form of bubbles. At 80 ^{o}C however, the overpotential under bubble-free conditions had declined quite notably to ~20 mV (Figure 9(a)). This is lower than previous reports[28] in which H_2 had been generated in the form of bubbles, even at elevated temperatures.

The overpotentials for O_2 generation at the Gortex-based $NiCo_2O_4$ anode were substantially larger than for H_2 generation. At 10 mA/cm^2, under bubble-free conditions, they were 0.31 V at 40 ^{o}C, 0.25 V at 60 ^{o}C, and 0.11 V at 80 ^{o}C (Figure 9(b)). By contrast, the overpotential of PTFE-bound $NiCo_2O_4$ at 10 mA/cm^2, when O_2 was generated in the form of bubbles, was previously measured in 5 N KOH to be:[35] ~0.34 V at 40 ^{o}C, ~0.29 V at 60 ^{o}C, and ~0.27 V at 80 ^{o}C. Thus, the overpotentials for bubble-free O_2 generation in Figure 9(b) are somewhat lower than the previously reported overpotentials for O_2 generation in the form of bubbles at 40 ^{o}C and more so at 60 ^{o}C. At 80 ^{o}C, it is drastically lower, being ~0.27 V with bubble formation but 0.11 V without bubble formation; a decline of 0.16 V.

In going from 40 ^{o}C to 80 ^{o}C, the overpotential of the $NiCo_2O_4$ catalyst for O_2 generation in the form of bubbles at 10 mA/cm^2, therefore declined in an incremental manner (namely, from ~0.34 V to ~0.27 V, which equates to an average 1.75 mV decrease per 1 ^{o}C increase in

temperature).[35] However, under bubble-free conditions with a Gortex substrate present at 10 mA/cm^2, it declined in an accelerating manner (namely, from 0.31 V to 0.11 V, which equates to an average 5 mV decrease per 1 ^oC increase in temperature). This fundamental difference is the main source of the effects noted above in the bubble-free electrolyzers. It correlates with the onset potentials of the Gortex-based electrolyzers (Figures 6-7), which also declined in an accelerating manner in going from 40 ^oC to $\geq$80 ^oC, whereas conventional, bubble-generating electrolyzers typically display an incremental decline.

Given that the Arrhenius equation predicts exponentially accelerating reaction rates as the temperature is increased, bubble formation is implied to interfere in some way with the smooth progression of the catalytic sequence. Such interference may, potentially, involve masking of the catalytic surface and/or the need to maintain high levels of gas supersaturation in the surrounding liquid electrolyte in order to nucleate and release a stream of bubbles. Such interferences may only allow incremental escalations in the catalytic rate with increasing temperature. Without such interferences – in a bubble-free system – more rapid accelerations in catalytic rate with increasing temperature may be possible.

This view is supported by work published during the drafting of this paper.[14] Chu and Cui at Stanford University reported electrocatalysis inspired by mammalian breathing processes, in which a $Au/NiFeO_x$ catalyst layer (50-100 nm thick) on a nano-porous polyethylene substrate (12 μm thick) generated O_2 without forming bubbles (up to 1.6 V vs RHE).[14] The catalysis, which was only demonstrated on a working electrode and not in an electrolyzer, produced a low overpotential of 190 mV at 10 mA/cm^2 under completely bubble-free conditions. Under partly bubble-generating conditions, with a ~400 μm thick, conventional carbon-PTFE gas diffusion layer, the overpotential was a higher 230 mV.[14] Under fully bubble- generating conditions, when the $Au/NiFeO_x$ was

(a)

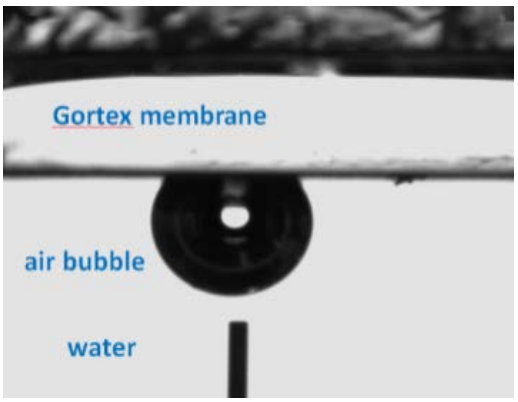

(b)

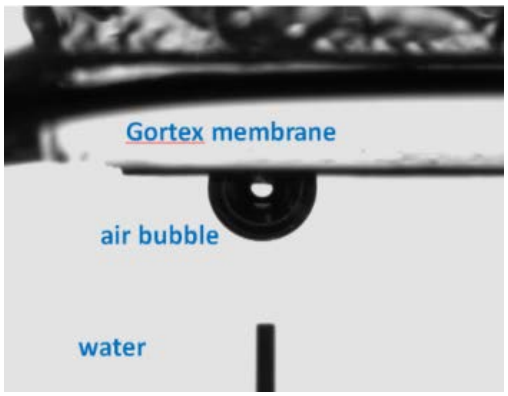

(c)

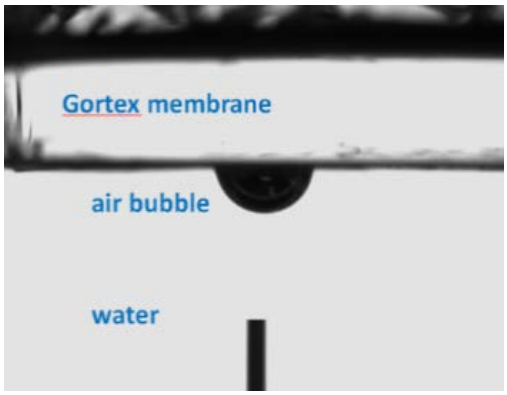

Figure 10. Interaction of an air bubble with a Gortex surface immersed in water. The back of the Gortex had a glass plate pushed tight up against it. In (a), an air bubble is placed on the Gortex surface facing the water. The Gortex thereafter rapidly drew the air bubble into it, as shown in (b) and then in (c). Within seconds, the air bubble was almost totally taken up by the Gortex.

deposited on a non-porous polyethylene substrate that had no capacity to directly take up newly-formed gases, the overpotential was 280 mV.[14] The authors ascribed the 0.09 V change in overpotential to "the additional energy" required to form and release gas bubbles.

2.9 The Mechanism of Gas Extraction by Gortex. Its Effect on Overall Efficiency. To examine the role of the Gortex in the above effects, we studied its interaction with gases in water.

As noted earlier, the ePTFE surface of Gortex comprises of hydrophobic PTFE micro-fibrils (Figure 2). Numerous previous studies have demonstrated that newly-formed gases, being also hydrophobic, selectively coalesce on PTFE surfaces.[36-41] For example, Ni electrodes with islands of PTFE on their surface, have been shown to generate gas bubbles on the PTFE islands before they do on the Ni at low voltages during water electrolysis.[36] PTFE surfaces are, indeed, said to *'scavenge'* gases dissolved in the surrounding aqueous electrolyte.[38,40] The first role of the Gortex therefore likely involves attracting and coalescing newly-formed gases on its PTFE surfaces.

Gortex is also highly porous. To examine the effect of this porosity on gas uptake, we studied the interaction of air bubbles with the surface of uncoated Gortex immersed in water. We used the "Captive Bubble" technique of contact angle measurement. Figure 10 (and Video S2) shows typical sequences of events when air bubbles were placed on or near to a horizontally-disposed Gortex membrane. The bubbles were rapidly drawn into the Gortex, even when a glass backing plate was pressed tight against the back of the Gortex to slow the process (Figure 10). When the backing plate was removed, air bubbles that touched the Gortex were instantly drawn into it.

To see whether the buoyancy of the bubbles played a role in this process, we turned the Gortex vertically in the water and again placed gas bubbles on its surface. Gravity and buoyancy

should cause such bubbles to rise vertically, parallel to or away from the Gortex. Instead, as shown in Video S3, the bubbles were quickly drawn into the Gortex in a horizontal motion.

These observation can be explained by a capillary action. Capillary pressures in porous materials are described by the Young-Laplace equation:

$$P_c = \frac{2\gamma}{r}\cos\phi \qquad \ldots(2)$$

where P_C = the capillary pressure, r = the pore radius, γ = the surface tension of the liquid, and ϕ = the contact angle of the material that forms the porous structure. The Gortex employed in this work had hydrophobic pores of 0.1 μm average radius. Its contact angle with the 6 M KOH electrolyte was measured to be 115°. The surface tension of 6 M KOH at 80 °C is 0.07511 N/m.[42]

Applying this data to equation (2) indicates that the capillary pressure of the Gortex was -634,857 N/m^2, which equates to -6.3 bar. The negative sign indicates only the direction of the capillary action; namely, it indicates that water is repelled by the pores whereas hydrophobic fluids (like gases) are attracted to and drawn into the pores.

The Gortex may therefore exert a strong capillary action that draws gases into it. This would particularly affect newly-formed gases that coalesce on its PTFE surfaces. Such gases may be continuously drawn into the Gortex before they are able to nucleate bubbles, thereby explaining the absence of observable bubbles during electrolysis.

Such a mechanism could explain why the effects noted above were also observed, albeit in less intense form in: (1) the Villa electrolyzer (Figure 8),[25] which employed conventional carbon-PTFE gas diffusion layers, and (2) in Cui and Chu's Au/NiFeO$_x$ catalyst deposited on a nano-porous polyethylene membrane.[14] The Gortex employed in this work had microscopic pores that

were smaller and more hydrophobic than the conventional carbon-PTFE gas diffusion layers in the Villa electrolyzer.[25] This imparted the Gortex electrodes with a more powerful capillary effect (and larger capillary pressure), resulting in an increased capacity for continuous gas extraction. In similar vein, the polyethylene in Cui and Chu's system[14] was also hydrophobic but less so than PTFE. This was partly compensated however, by the presence of nanoscopic pores that were smaller on average than the microscopic pores of the Gortex. A capacity to scavenge newly-formed gases that coalesce on the polyethylene surface, coupled with a 'gas-philic' capillary action, clearly also existed in that system.

The capacity of the Gortex to continuously de-gas its adjoining catalyst layer should strongly affect the extent to which the electrolyte in the catalyst layer is supersaturated with dissolved gas. The more rapidly this de-gassing occurs, the lower the average level of supersaturation may be expected to be. In a bubble-generating system by contrast, the catalyst layer must always be highly supersaturated with dissolved gas in order to continuously nucleate and release a stream of bubbles. The lowered onset potentials of the bubble-free electrolyzers may reflect the fact that additional voltage is not needed to create and maintain this high level of supersaturation. Such additional voltage may, in fact, comprise the *bubble overpotential* that was discussed earlier.

In effect, the Gortex provides a more efficient route for mass transport of product gases away from the electrodes than is available in conventional, bubble-generating electrolyzers. This manifests in greater intrinsic efficiency, with low onset potentials and diminished electrode overpotentials.

2.10 The Energy Efficiency Penalty due to Bubble Formation and Release. The energy penalty associated with the need to form bubbles in an electrolyzer may be estimated by comparing the η^{act}_{cell} at 80 ^{o}C, of the conventional, bubble-forming electrolyzers in Figure 1 ($\eta^{act}_{cell} \geq 0.27$ V) with the bubble-free electrolyzer in Figure 6 (iR-corrected η^{act}_{cell} 0.09 V). Even if a generous iR-correction of 0.02 V is applied to the electrolyzers in Figure 1, giving them an iR-corrected η^{act}_{cell} $\geq$0.25 V, the bubble-free electrolyzer still commences gas production at a voltage that is 0.16 V lower than the bubble-generating electrolyzers. This 0.16 V represents the bubble overpotential when the influence of impedance is excluded.

Under endothermic conditions, the point of 100% efficiency in an electrolyzer may best be considered to be E^{o} (1.183 V at 80 ^{o}C).[1] This voltage represents 100% efficiency in respect of the Lower Heating Value (LHV) of hydrogen. An additional requirement of 0.16 V then decreases the maximum available energy efficiency in an electrolyzer to: 1.183/(0.160+1.183) x 100 = $\leq$88.1% LHV. That is, the decrease in energy efficiency in the electrolyzer due to bubble formation and release is estimated to be $\geq$11.9% (LHV).

3. CONCLUSION AND FUTURE PERSPECTIVES

This work has described novel, bubble-free water electrolyzers that utilize Gortex-based electrodes to achieve unprecedented intrinsic efficiency, as demonstrated by their remarkably low onset potentials at $\geq$80 ^{o}C.

Electrolyzer polarization curves are governed by two critical features: the onset potential and the ohmic slope. The ohmic slope is determined by the impedance of the cell, which is mostly set by its architecture and engineering. This can be fairly readily optimized. The onset potential is,

however, determined by the catalytic mechanisms within the electrolyzer, which are less readily optimized. A highly efficient electrolyzer of the future, will necessarily combine the lowest possible onset potential (highest inherent efficiency) with the smallest (flattest) possible ohmic slope (lowest impedance), as depicted in Figure S7.

Beyond the fundamental insights that the above, impedance un-optimized bubble-free electrolyzers impart, they also highlight a possible pathway to very low onset potentials. To develop a highly efficient electrolyzer of the future that was efficient at all current densities however, they would have to be impedance optimized to thereby realize the smallest possible ohmic slope.

ACKNOWLEDGEMENTS

The authors acknowledge support under Australian Research Council (ARC) Linkage Grant LP130101135 and from industry partner, AquaHydrex Pty Ltd. PT acknowledges an ARC Post-Graduate Award. Support from the ARC Centre of Excellence Scheme (Project CE140100012) is acknowledged. The use of facilities within the University of Wollongong Electron Microscopy Centre funded by ARC Linkage, Infrastructure, Equipment and Facilities grant LE160100063 is acknowledged. The Australian National Fabrication Facility (ANFF) Materials node is acknowledged for design and printing of custom-parts.

DECLARATION OF INTERESTS

Portions of this work are drawn from the PhD thesis of PT. GT and GFS declare part-time work with the industry partner for the grant that funded this work.

REFERENCES

(1) (a) Jensen, J. O.; Bandur, V.; Bjerrun, N. J.; Jensen, S. H.; Ebbesen, S.; Mogensen, M.; Trophoj, N.; Yde, L. *Pre-Investigation of Water Electrolysis*, Publication PSO-F&U 2006-1-6287, RISO and the Danish Technical University, 2008, and references therein. (b) Godula-Jopek, A. *Hydrogen Production by Electrolysis*, Wiley-VCH, 2015, and references therein. (c) Zuettel, A.; Remhof, A.; Borgschulte, A.; Friedrichs, O. *Phil Trans R. Soc.* **2010**, *368*, 3329-3342. (d) Zheng, K.; Zhang, D. *Prog. Energy Combust. Sci.* **2010**, *36*, 307-326. (e) Schalenbach, M.; Zeradjanin, A. R.; Kasian, O.; Cherevko, S.; Mayrhofer, K. J. J. *Int. J. Electrochem. Sci.* **2018**, *13*, 1173-1226.

(2) For an electrolyzer powered by a solar array, see, for example: Schiller, G.; Henne, R.; Mohr, P.; Peinecke, V. *Int. J. Hydrogen Energy* **1998**, *23*,761-765.

(3) Brimblecombe, R.; Chen, J.; Wagner, P.; Buchhorn, T.; Dismukes, G. C.; Spiccia, L.; Swiegers, G. F. *J. Molec. Catal. A Chem.* **2011**, *338*, 1-6, and references therein.

(4) See, for example: Mandin, P.; Derhoumi, Z.; Roustan, H.; Wuethrich, R. *Electrochim. Acta* **2014**, *128*, 248-258.

(5) See, for example: Maljusch, A.; Ventosa, E.; Rincon, R. A.; Bandarenka, A. S.; Schuhmann, W. *Electrochem. Commun*. **2014**, *38*, 142-145.

(6) Hug, W.; Divisek, J.; Mergel, J.; Seeger, W.; Steeb. H. *Int. J. Hydrogen Energy* **1992,** *17*, 699-705.

(7) Lewinski, K.; Sun, F.; Luopa, S.; Park, J.; Masel, R. *Operation of Low-Temp Electrolyzers at Very High Current Densities: A Pipe Dream or An Opportunity*.

Presentation number 52 at the 1st International Conference on Electrolysis, Copenhagen, June 13-15, 2017 (www.ice2017.net/conference/presentations).

(8) Ioroi, T.; Okub, T.; Yasuda, K.; Kumagai, N.; Miyazaki, Y. *J. Power Sources* **2003**, *124*, 385-389.

(9) Hamdan, M. *PEM Electrolyzer Incorporating an Advanced, Low Cost Membrane*. Presentation for Project PD030, Department of Energy Hydrogen Program Review, 2013 (www.hydrogen.energy.gov/pdfs/review13/pd030_hamdan_2013_o.pdf)

(10) Bernt, M.; Siebel, A.; Gasteiger, H. A. *J. Electrochem. Soc.* **2018**, *165*, F305-F314.

(11) Kraglund, M. R.; Caro, M.; Ali, D.; Schiller, G.; Christensen, E.; Friedrich, A.; Stolten, D.; Jensen, J. O. *Alkaline Membrane Electrolysis with PEM-level Electrochemical Performance.* Presentation number 59 at the 1st International Conference on Electrolysis, Copenhagen, June 13-15, 2017 (www.ice2017.net/conference/presentations).

(12) Nafion conductivity: Schalenbach, M.; Lueke, W.; Lehnert, W.; Stolten, D. *Electrochim. Acta* **2016**, *214*, 362-369; Alkaline membrane conductivity: see Vermeiren, P.; Adriansens, W.; Moreels, J. P.; Leysen, R. *Int. J. Hydrogen Energy* **1998**, *23*, 321-324. KOH conductivity: Gilliam, R. J.; Graydon, J.W.; Kirk, D. W.; Thorpe, S. J. *Int. J Hydrogen Energy* **2007**, *32*, 359. H_2SO_4 conductivity: Darling, H. E. J. *Chem. Eng. Data* **1964**, *9*, 421.

(13) Phillips, R.; Dunill, C. W. *RSC Advances* **2016**, *6*, 100643-100651.

(14) Li, J.; Zhu, Y.; Chen, W.; Lu, Z.; Xu, J.; Pei, A.; Peng, Y.; Zheng, X.; Zhang, Z.; Chu, S.; Cui, Y. *Joule* **2019**, *3*, 557-569.

(15) Shibata, S. *Electrochim. Acta* **1978**, *23*, 619-623.

(16) Wikol, M.; Hartmann, B.; Brendle, J.; Crane, M.; Beuscher, U.; Brake, J.; Shickel, T. Chap 23 in *Filtration and Purification in the Biopharmaceutical Industry, Second Edition* (Eds. Jornitz, M. W.; Meltzer, T. H.), Taylor & Francis, 2007.

(17) AlMarzooqi, F. A.; Bilad, M. R.; Mansoor, B.; Arafat, H. A. *J. Mater. Sci.* **2016**, *132*, 42359.

(18) Tiwari, P.; Tsekouras, G.; Swiegers, G. F.; Wallace, G. G. *ACS Appl. Mater. Interfaces* **2018**, *10*, 28176-18186.

(19) See, for example: Pashley, R. M.; Pashley, L. R. *Increased Conductivity and Enhanced Electrolytic and Electrochemical Processes. International Patent Appication* **WO 2006/066345**, and references therein.

(20) Winther-Jensen, O.; Chatjaroenporn, K.; Winther-Jensen, B.; MacFarlane, D. R. *Int. J. Hydrog. Energy* **2012**, *37*, 8185-8189.

(21) Wagner, K.; Tiwari, P.; Swiegers, G. F.; Wallace, G. G. *Adv. Energy Mater.* **2018**, *8*, 1702285.

(22) Wagner, K.; Tiwari, P.; Swiegers, G. F.; Wallace, G. G. *Energy Environ. Sci.* **2018**, ***11***, 172-184.

(23) Winther-Jensen, B.; Winther-Jensen, O.; Forsyth, M.; MacFarlane, D. R. *Science* **2008**, *321*, 671-674.

(24) Kolodziejczyk, B.; Winther-Jensen, O.; Pereira, B. A.; Nair, S. S.; Winther-Jensen, B. *J. Appl. Polymer Sci.* **2015**, *132*, 42359.

(25) Marini, S.; Salvi, P.; Nelli, P.; Pesenti, R.; Villa, M.; Berrettoni, M.; Zangari, G.; Kiros, Y. *Electrochim. Acta* **2012**, *82*, 384-391.

(26) Jonville, P. *Electrolyzer with Released Gas. US Patent 4,086,155*.

(27) See, for example: German, S. R.; Edwards, M. A.; Chen, Q.; White, H. S. *NanoLett*. **2016**, *16*, 6691-6694, and references therein.

(28) Kraglund, M. *Alkaline Membrane Water Electrolysis with Non-Noble Catalysts*, PhD Thesis, Danish Technical University, 2017, and references therein; see p. 36-37 for a summary of previously reported hydrogen overpotential, p. 44-45 for a summary of previously reported oxygen overpotentials, and p. 54 (Fig. 2.9) for a compilation of hydrogen and oxygen solubilities in KOH.

(29) Diffusion co-efficients for oxygen and hydrogen gas in KOH can be found in: Tham, M. K.; Walker, R. D.; Gubbins, K. E. *J. Phys. Chem.* **1970**, *74*, 1747-1751.

(30) Diffusion co-efficients for oxygen gas in KOH that confirm those in the previous reference can be found in: Lu, Y.-Q.; Li, S.-H.; Wang, S.-N.; Du, H.; Zhang, Y. *Acta Phys. Chem. Sinica* **2015**, *31*, 1045-1053.

(31) For example: Schalenbach, M.; Carmo, M.; Fritz, D. L.; Mergel, J.; Stolten, D. *Int. J. Hydrogen Energy* **2013**, *38*, 14921-14933.

(32) For example: Schalenbach, M.; Lueke, W.; Stolten, D. *J. Electrochem. Soc*. **2016**, *163*, F1480-F1488.

(33) For example: Schalenbach, M.; Tjarks, G.; Carmo, M.; Lueke, W.; Mueller, M.; Stolten, D. *J. Electrochem. Soc*. **2016**, *163*, F3197-F3208.

(34) Bratsch, S. G. *J. Phys. Chem. Ref. Data* **18**, 1-21 (1989).

(35) Jasem, S. M.; Tseung, A. C. C. *J. Electrochem. Soc. Electrochem. Sci. Tech*. **1979**, *126*, 1353-1360

(36) Brussieux, C.; Viers, Ph.; Roustan, H.; Rakib, M. *Electrochim. Acta* **2011**, *56*, 7194-7201.

(37) Tseung, A. C. C.; Vassie. P. R. *Electrochim. Acta* **1976**, *21*, 315-318.

(38) Teschke, O.; Galembeck, F. *J. Electrochem. Soc. Electrochem. Sci. Tech*. **1983**, *130*, 33-36.

(39) Sequeira, C. A. C.; Santos, D. M. F.; Sljukic, B.; Amaral, L. *Braz. J. Phys.* **2013**, *43*, 199-208.

(40) Kadyk, T.; Bruce, D.; Eikerling, M. *Sci. Reports* **2017**, 6, 38780 (DOI: 10.1038/srep38780)

(41) Sides, P. J.; Tobias, C. W. *J. Electrochem. Soc. Electrochem. Sci. Tech.* **1985**, *132*, 583-587.

(42) Ripoche, P.; Rolin, M. *Bull. Soc. Chim. France Part. I **1980**, 9-10, I386–I39.*

(43) Tawfik, M. E.; Diez, F. J. *Electrochemica Acta* **2014**, *146*, 792-797.

(44) Ren, H.; German, S. R.; Edwards, M. A.; Chen, Q.; White, H. S. *J. Phys. Chem. Lett.* **2017**, *8*, 2450-2454.